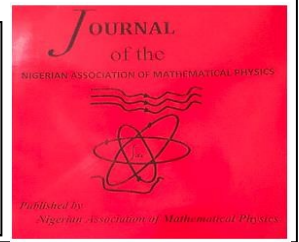


The Nigerian Association of Mathematical Physics

Journal homepage: <https://nampjournals.org.ng>



Kinematic Wave Speed of Flow-Density Models of Vehicular Traffic Flow

*Mabur Yaks Mafuyai, Dirting Dakup Bakwa and Yakubu Yerima Jabil

Department of Physics, Faculty of Natural Sciences, University of Jos.

<https://doi.org/10.60787/jnamp-v67i1-342>

ARTICLE INFO

Article history:

Received xxxxx

Revised xxxxx

Accepted xxxxx

Available online xxxxx

Keywords:

Kinematic wave
model,

Fundamental diagram

Kinematic wave speed,

Flow-density model,

Shock wave.

ABSTRACT

Kinematic wave speed represents the propagation of information within traffic states. How well equilibrium functional form of an empirical fundamental diagram predicts this parameter determines how well a kinematic wave model replicates observed traffic phenomena during simulation. In the light of this, we investigated the kinematic wave speed prediction of some selected functional forms of an empirical fundamental diagram. GA400 data was used to calibrate the models and assess their fitting accuracy. The first derivatives of the selected models were plotted against density, and the predicted jam density for each model was substituted into its derivative to determine its kinematic wave speed at jam. The results show that the newly proposed model [14] produces the most likely kinematic wave speed observe on GA400 highway followed the model [2 and 17] respectively. These result shows that the proposed model could be more suitable for dynamic analysis using kinematic wave model.

1.0 Introduction

Kinematic wave speed is an important dynamic parameter in dynamic analysis of traffic flow using continuum models. The kinematic wave speed originated from the kinematic wave model of Lighthill-Whitham-Richard given by eqn. (1) & (2). It is the speed at which small disturbances (Traffic information) propagate within a traffic stream. It can be thought of as the limiting case of shock wave speed when the difference in densities of the two traffic states approaches zero.

$$\frac{\partial k(x, t)}{\partial t} + \frac{\partial q(x, t)}{\partial x} = 0 \quad (1)$$

$$q = Q(k) \quad (2)$$

*Corresponding author.: Mabur Yaks Mafuyai.

E-mail address: mafuyaim@unijos.edu.ng

1118-4388 © 2024 JNAMP. All rights reserved

Where, k and q are traffic density and flow respectively.

Eqn. (2) which is called equilibrium fundamental diagram is deduced from the fundamental equation of traffic expressed as eqn. (3) by assuming speed, $v(x, t)$ to be a function of density, $k(x, t)$ only.

$$q = k(x, t)v(x, t) \tag{3}$$

Substituting eqn. (2) in eqn. (1) leads to eqn. (4) given as:

$$\frac{\partial k(x, t)}{\partial t} + \frac{dq}{dk} \frac{\partial q(x, t)}{\partial x} = 0 \tag{4}$$

Eqn. (4) has a solution of the form:

$$k(x, t) = F(x - ct, t) \tag{5}$$

With F being any arbitrary function and c given as:

$$c = \frac{dq}{dk} \tag{6}$$

Eqn. (6) is the kinematic wave speed. It can be seen that kinematic wave speed is the first derivative of eqn. (2), the equilibrium fundamental diagram. Its value depends on the equilibrium fundamental diagram. Therefore, how accurate the functional form of any equilibrium fundamental diagram fits a given empirical fundamental diagram determines how well the kinematic wave model replicates the dynamics of the given traffic flow. It is in the light of this, that this research aims to investigate the kinematic wave speed of selected functional forms of equilibrium fundamental diagrams. The rest of the paper is organized as follows, section 2 provide the literature review on some selected fundamental diagram models, section 3 outlines the methodologies employed in the study, section 4 presents the findings, and section 5 presents the results discussion and conclusion.

An explicit form of eqn. (2) started with the work of [1] and since then, tones of other functions have been proposed. This is owing to the importance of fundamental diagram in traffic flow management, control and analysis; and lack of a single successful model that accurately describe traffic states within all density range. Literature has shown that existing functional forms of the equilibrium fundamental diagram perform poorly at mid and high densities. And, it is believed that it is at these density ranges that most interesting traffic phenomena arise [2], [3], [4].The debate as to whether the empirical fundamental diagram can be described accurately by a single function or multiple functions representing different regions on the empirical fundamental diagram has remain active for many decades now. The lack of consensus among researchers is due to inability of any previously proposed model to consistently represent accurately the traffic states at all densities. This has led to two schools of thoughts - those that believe the fundamental diagram is continuous and hence can be represented by a single function [5,6] and those that believe that discontinuity exist and hence, there is the need for two or more functions [7,8,9] to correctly represent empirical fundamental diagram.

Single-Regime fundamental diagrams are fundamental diagrams represented by a single mathematical expression. Their greatest attraction is mathematical elegance. Some of the recently proposed single-regime models include Five-Parameter logistic model by [10], longitudinal control model by [11], and models by [12], [13], [2], [14]. Multi-regime fundamental diagram on the other hand requires two or more mathematical functions to correctly represent empirical fundamental diagram. [8] was the first to propose a multi-regime fundamental diagram. Two mathematic functions were used in his work – Greenberg

logarithmic function [15] used to describe congestion regime and Underwood exponential function [16] used to describe free-flow regime. Since the work of Edie, many more multi-regime models have been proposed for various purposes. Two of these models that are investigated in this research are presented in Table 1 alongside some selected single-regime models.

Table 1
Some Selected Single-regime and Multi-regime Models

Author(s)	Functional Form	Parameters
[17]	$q = \frac{v}{c_1 + \frac{c_2}{V_f - v} + c_3 v} \quad \text{or}$ $q = \alpha (1 - \beta k - ((\gamma k - 1)^2 + \delta k^2)^{1/2}) \quad \text{Brahmic et al, (2022)}$	V_f, c_1, c_2, c_3 $\alpha, \beta, \gamma, \delta$
[10]	$q = k \left(V_b + \frac{V_f - V_b}{[1 + \exp(\frac{k - k_t}{\theta_1})]^{\theta_2}} \right)$	$V_f, V_b, k_t, \theta_1, \theta_2$
[13]	$q = V_f k \frac{(1 - (\frac{k}{k_j})^a)^b}{1 + E (\frac{k}{k_j})^\theta}$	$V_f, E, k_j, \theta, a, b$ Parameter b was fixed at 1
[13]	$q = V_f k \frac{(e^{-\frac{k}{k_c} (1+a)} - e^{-\frac{k_j}{k_c} (1+a)})^b}{1 - e^{-\frac{k_j}{k_c} (1+a)}}$	V_f, k_c, k_j, a, b Parameter b was fixed at 1.
[2]	$q = \frac{V_f k}{[1 + (\frac{k}{k_c})^m]^{2/m}}$	V_f, k_c, m
Proposed [14]	$q(k) = V_f k [0.35 (1 - (g(k))^{n-1}) + 0.65 \{1 - (g(k))^{n-1}\}^{2n}]$ $g(k) = 1 - \frac{1.2(k_j^n - k^{n-1} k_j)}{(1.2^{1/n} k_j + k)^n}, \quad \forall n \in \mathcal{R}: n > 1$	V_f, k_j, n
[8]	$q = \begin{cases} V_f k \exp^{-\frac{k}{k_m}} & k < k_b \\ V_m k \ln \frac{k_j}{k} & k \geq k_b \end{cases}$	V_f, k_m, V_m, k_j, k_b
[7]	$q = \begin{cases} V_f k - c k^2 & k \leq k_b \\ v_{bw} k - (\frac{v_{bw}}{k_j}) k^2 & k > k_b \end{cases}$	V_f, c, v_{bw}, k_j, k_b

2. Methodology

2.1 Models selection

The equilibrium functional forms of empirical fundamental diagram selected for this study and given in Table 1 were selected on the following basis: 1. The Edie multi-regime model, Drake et al.’s two-regime model, Wang et al five-parameter logistic model, and van Aerde model were selected because of their performance ranking according to the comprehensive comparison study by [18], [19]. 2. The remaining models considered in this research were selected because they are relatively new and were not covered in the comparative study by [18, 19].

2.2 Model Calibration

GA400 data set was used for the calibration because it is fairly complete. It has data points in all operational state of traffic. Least square technique was used via Levenberg-Marquardt algorithm in python. Fitting accuracy was determined using the error metrics presented in eqns. (7), (8), and (9).

$$\text{Mean square error (MSE)} = \frac{1}{N} \sum_{i=1}^N (y_{ei}(k) - y_{mi}(k))^2 \tag{7}$$

$$\text{Root mean square error (RMSE)} = \sqrt{\frac{1}{N} \sum_{i=1}^N (y_{ei}(k) - y_{mi}(k))^2} \tag{8}$$

$$\text{Average Relative Error (ARE)} = \frac{1}{N} \sum_{i=1}^N \frac{|y_{ei}(k) - y_{mi}(k)|}{|y_{mi}(k)|} \tag{9}$$

$y_{ei}(k)$, $y_{mi}(k)$, and N are experimental or observed values, model’s predicted values, and number of data points respectively. These are preferred because they are the most common used metrics to measure fitness statistically.

2.3 Kinematic wave speed determination

To determine the kinematic wave speed, first derivative of all the selected models were determined (Table 2) and graphed against density. Kinematic wave speed at jam density was determined for models that predict jam density by substituting the values of jam density predicted.

Table 2

First and Second Derivatives of the Models being compared

Model	Derivatives	
Proposed [14]	First	$q' = V_f [0.35(1 - (g)^{n-1}) + 0.65 \{1 - (g)^{n-1}\}^{2n}] - V_f k(n-1)g'(g)^{n-2} [0.35 + 1.3n \{1 - (g)^{n-1}\}^{2n-1}]$
		$g'(k) = \frac{1.2(n-1)k_j k^{n-2} + 1.2n(k_j^n - k^{n-1}k_j)(1.2^{1/n}k_j + k)^{-1}}{(1.2^{1/n}k_j + k)^n}$ $g(k) = 1 - \frac{1.2(k_j^n - k^{n-1}k_j)}{(1.2^{1/n}k_j + k)^n}$
Wang SPL	First	$q'(k) = (V_b + \frac{V_f - V_b}{[1 + \exp(\frac{k - k_t}{\theta_1})]^{\theta_2}}) - k \frac{(V_f - V_b)\theta_2 \exp(\frac{k - k_t}{\theta_1})}{\theta_1 [1 + \exp(\frac{k - k_t}{\theta_1})]^{\theta_2 + 1}}$

Modified Lee	First	$q'(k) = V_f \frac{(1 - (a + 1) \left(\frac{k}{k_j}\right)^a)}{1 + E \left(\frac{k}{k_j}\right)^\theta} - \frac{V_f E \theta (k^\theta - \frac{k^{a+\theta}}{k_j^{\frac{a+\theta}{a}}})}{(1 + E \left(\frac{k}{k_j}\right)^\theta)^2}$
Gaddam & Rao	First	$q'(k) = \frac{V_f \left(e^{-\left(\frac{k}{k_c}\right)^{(1+a)}} - (1+a) \left(\frac{k}{k_c}\right)^{(1+a)} e^{-\left(\frac{k}{k_c}\right)^{(1+a)}} - e^{-\left(\frac{k_j}{k_c}\right)^{(1+a)}} \right)}{1 - e^{-\left(\frac{k_j}{k_c}\right)^{(1+a)}}$
Cheng et al.		$q'(k) = \frac{V_f}{\left[1 + \left(\frac{k}{k_c}\right)^m\right]^{2/m}} - \frac{2V_f \frac{k}{k_c} \left(\frac{k}{k_c}\right)^{m-1}}{\left[1 + \left(\frac{k}{k_c}\right)^m\right]^{2/m+1}}$
Edie	First	$q'(k) = \begin{cases} V_f \left(1 - \frac{k}{k_m}\right) \exp\left(-\frac{k}{k_m}\right) & k < k_b \\ V_m \left(\ln \frac{k_j}{k} - 1\right) & k \geq k_b \end{cases}$
Drake	First	$q'(k) = \begin{cases} V_f - 2ck & k \leq k_b \\ v_{bw} - 2 \left(\frac{v_{bw}}{k_j}\right) k & k > k_b \end{cases}$
Van Aerde	First	$q'(k) = \alpha \left(-\beta - \left((\gamma k - 1)^2 + \delta k^2 \right)^{-1/2} \left((\gamma k - 1) \gamma + \delta k \right) \right)$

3. Results

The results of this research are presented in charts, graphs, and tables for compactness, easy reference, and clarity. Firstly, the calibration results are presented, Fig. 1 & 2, and Table 3. These explain the fitting accuracy of each model. Lastly, the kinematic wave speed results are presented in Fig. 3 and table 4.

3.1 Calibration Results

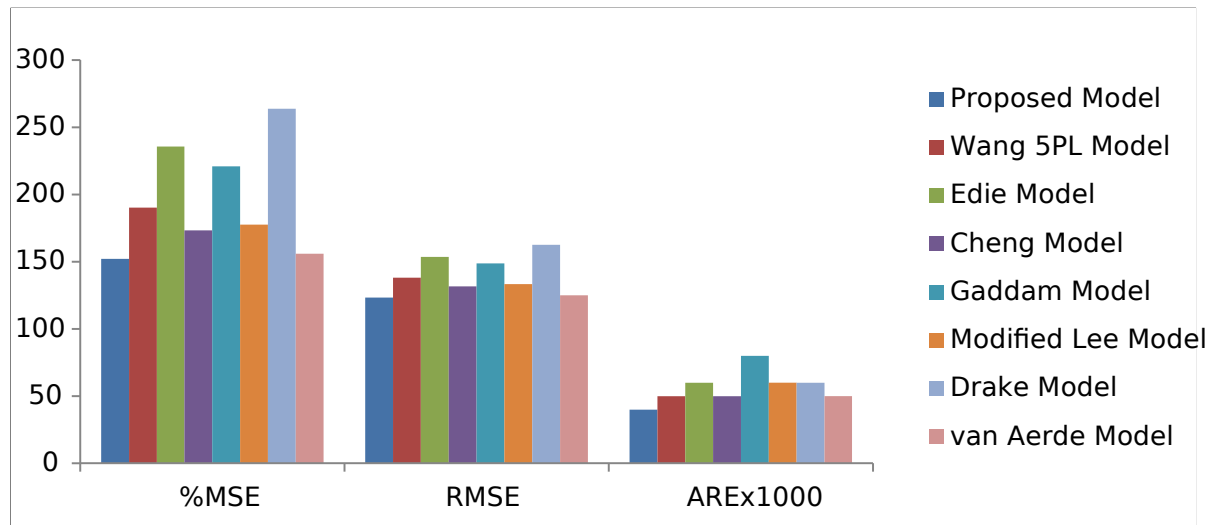


Figure 1 Group bar chart of the statistical metrics used to measure model fitness to empirical data

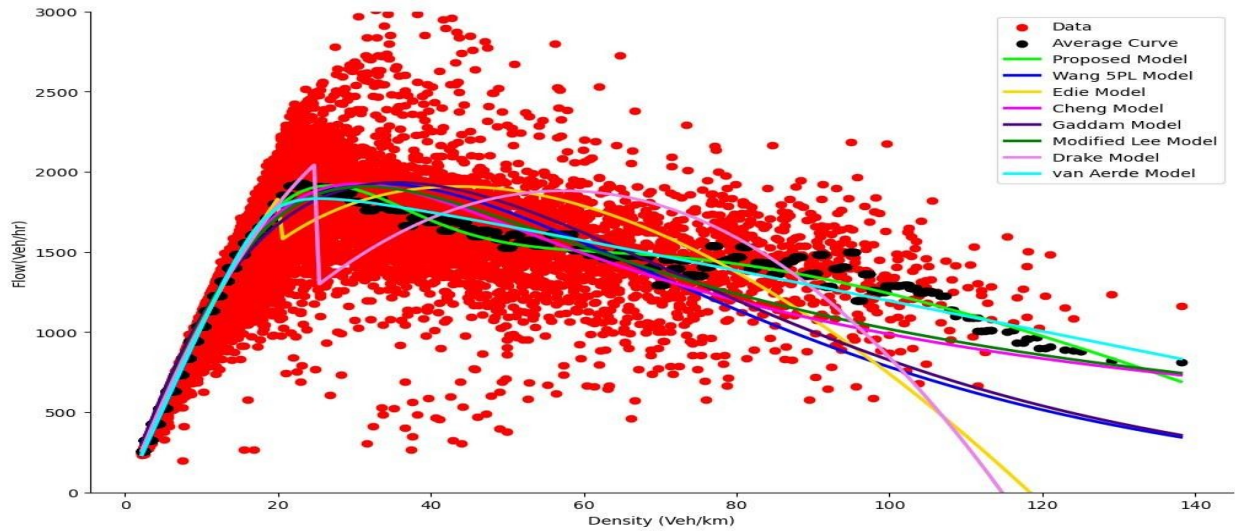


Fig. 2. Graph of the optimized models and average curve of the GA400 data

Table 3

Estimates of the parameters using LM algorithm and GA400 data

Models	Parameters	Parameter	Values			
Proposed Model	Parameters	V_f	k_j	n		
	Initial	100.00	160.00	4.00		
	Optimized	105.76	176.89	5.31		
Wang 5PL Model	Parameters	V_f	V_b	k_t	θ_1	θ_2
	Initial	104.00	9.00	17.00	2.10	0.07
	Optimized	103.49	9.00	13.90	1.29	0.04
Edie Multi-Regime Model	Parameters	V_f	V_c	k_c	k_j	k_b
	Initial	104.00	65.00	30.00	175.00	20.00
	Optimized	118.96	43.83	76.27	118.73	20.00
Cheng Model	Parameters	V_f	k_c	m		
	Initial	105.00	65.00	4.00		
	Optimized	111.45	30.40	2.45		
Gaddam Model	Parameters	V_f	k_j	k_c	a	
	Initial	105.00	179.00	65.00	0.60	
	Optimized	138.95	820.27	37.75	0.07	
Modified Lee Model	Parameters	V_f	k_j	E	θ	a
	Initial	105.00	179.00	10.30	2.14	4.00
	Optimized	115.59	151.60	24.87	2.11	131.83

Drake Two Regime Model	Parameters	V_f	k_j	k_b	c	v_{bw}
	Initial	105.00	80.00	25.00	5.00	-15.00
	Optimized	120.26	114.72	25.00	1.52	65.62
van Aerde Model	Parameters	α	β	γ	δ	
	Initial	1000.00	0.007	0.050	0.5000	
	Optimized	1098.56	-0.044	0.051	0.0002	

3.2 Kinematic wave speed Results

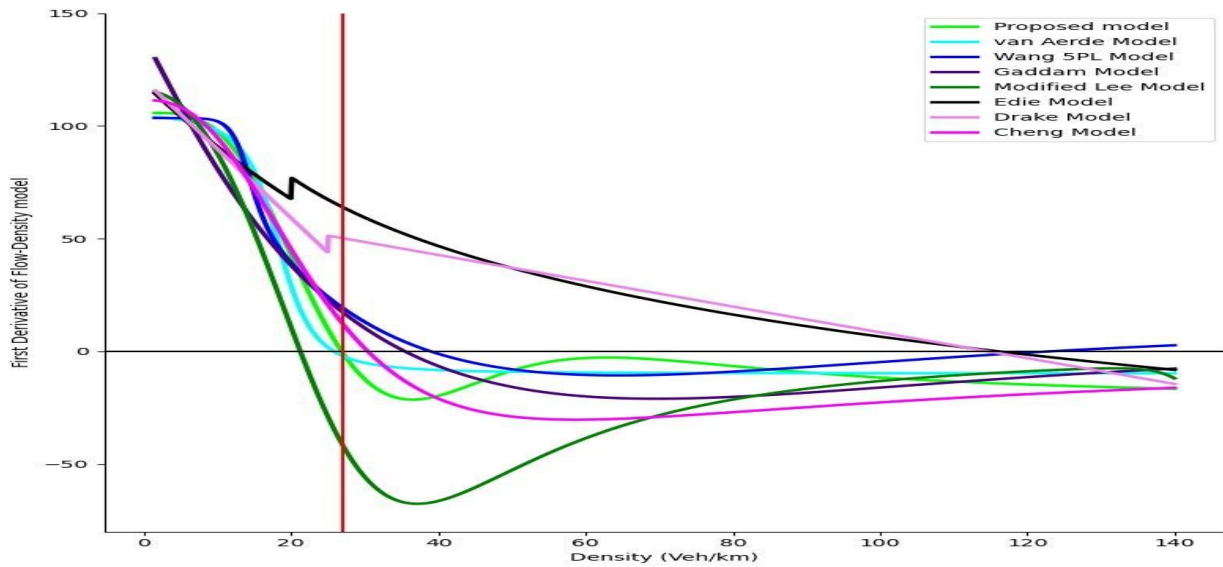


Fig. 3. Graphs of first derivatives against density of the compared models

Table 4

Predicted Kinematic Wave Speeds at Jam density for GA400 ITS data set

S/n	Model	Kinematic Wave Speed (km/hr)
1	Proposed Model	-19.50
2	Wang 5PL Model	Nil
3	Edie Multiple Regime Model	-13.96
4	Cheng Model	Nil
5	Gaddam Model	-5.9×10^{-9}
6	Modified Lee Model	-221.04
7	Drake Two Regime Model	-65.62
8	van Aerde Model	-9.79

Note: Nil indicates that the model does not estimate kinematic wave speed

4. Discussion

From Fig. 1, it can be observed that the proposed model has the least error, irrespective of the error metric, followed by the models of van Aerde and Cheng et al. respectively. This clearly shows that the proposed model [14] fits GA400 data better. Furthermore, Fig. 2 shows that the proposed model could predict the equilibrium traffic state more accurately across all the branches of traffic operation – free-flow, transition, and congestion branch. While van Aerde’s model shows relatively good performance in this aspect, it appears to under estimate the equilibrium capacity and speed at high densities. All the other models over estimate the traffic states at mid densities and under estimate the traffic states at high densities. Table 3 gives the parameters estimate of the models. It can be observed that all the models predict free-flow speed values that are within the observed range of values [10] and those that can predict jam density equally estimates acceptable values except the model of Gaddam and Rao that predicted unrealistic values. This result therefore implies that the kinematic wave speeds that the proposed model predicts could reflect the actual kinematic wave speeds observed on GA400 highway.

Fig. 3 gives the first derivative of the flow-density functional forms of the models against density. It can be observed that all the models have positive rates before the predicted critical densities and negative rates after the critical densities. This shows that the functions are monotone increasing at the right branch of the flow-density curve up to capacity and monotone decreasing on the left branch up to jam density [2]. The proposed model predicts a critical density of 27veh/km and the [17], [13] and [2] models equally predicts critical density values of 26veh/km, 21.5veh/km, and 31.5veh/km respectively. These values are closed to that of the proposed model and also appear realistic when observed from Fig. 2. Every other model predicts an unrealistic value, particularly the multi-regime models. The kinematic wave speed for densities less the critical densities is positive i.e. the positive quadrant of Fig 3. This means that small disturbances travel in the direction of the traffic flow. However, beyond the critical densities, the kinematic wave speed is negative implying that small disturbances travel against the direction of travel of traffic flow.

Given that the proposed model produces the correct kinematic wave speeds owing to its fitting accuracy as discussed above, the model with the next good performance is van Aerde’s model going by Fig. 3. This is not surprising as the model is the next most accurately fitted after the proposed model. However, after the critical density the model appears to predict a constant kinematic wave speed which is unrealistic. The trend of kinematic wave speed of the proposed model is worth noting. Immediately after critical density, the kinematic wave speed falls rapidly until it reaches minimum and then begins to increase again for some densities and thereafter, falls again steadily. This trend is consistent with field and simulation observation and the microscopic basis for this is some sequences of acceleration, deceleration, and car-following processes leading to possibly different capacities [3]; hence the appearance of the reverse lambda shape of which the proposed model clearly captures (Fig. 2). Similarly, the modified Lee’s models seems to follow the same trend, kinematic wave speed only begins to fall again after increasing far away from critical density which implies that reversed lambda shape is formed far away from capacity and this is unrealistic. Lastly, the trend of Wang et al.’s model is interesting as well. The model’s kinematic wave speed increases until it becomes positive at some high densities. This is completely awkward because this implies that drivers ahead receive information from those behind contrary to the unidirectional flow of information across traffic particles. This may be connected to the undesirable backward-bending phenomenon of the model at high densities as observed by some authors [2], [20].

The proposed model predicts a kinematic wave speed at jam of about -19.5km/hr annotated by the red line. This kinematic wave speed’s value falls within the observed range for United States[2]. Moreover, all the

models apart from the proposed model predict kinematic wave speed at jam outside the narrow range of -18km/hr to -20km/hr observed in the United State.

Conclusion

The kinematic wave speed prediction of some selected functional forms of an empirical fundamental diagram has been investigated and compared in the light of their fitting accuracy. Proposed model [14] predicts more realistic kinematic wave speeds at all densities followed by van Aerde's model and Cheng et al's models respectively. These shows that these models are likely to replicate field observation better during simulation using kinematic wave model.

References

1. B.D. Greenshields, "A study of traffic capacity," *Proc Highw. Res Board*, vol. 14, pp. 448–477, 1935.
2. Q. Cheng, Z. Liu, Y. Lin, and X. (Simon) Zhou, "An s-shaped three-parameter (S3) traffic stream model with consistent car following relationship," *Transp. Res. Part B Methodol.*, vol. 153, pp. 246–271, Nov. 2021, doi: 10.1016/j.trb.2021.09.004.
3. D. Ni, "Field Theory for Some Traffic Phenomena and Fundamental Diagram," *Transp. Res. Rec. J. Transp. Res. Board*, vol. 2675, no. 9, pp. 1195–1208, Sep. 2021, doi: 10.1177/03611981211006422.
4. X. Qu, S. Wang, and J. Zhang, "On the fundamental diagram for freeway traffic: A novel calibration approach for single-regime models," *Transp. Res. Part B Methodol.*, vol. 73, pp. 91–102, Mar. 2015, doi: 10.1016/j.trb.2015.01.001.
5. M. J. Cassidy, "Bivariate relations in nearly stationary highway traffic," *Transp. Res. Part B Methodol.*, vol. 32, no. 1, pp. 49–59, 1998, doi: 10.1016/S0191-2615(97)00012-X.
6. J. M. Del Castillo and F. G. Benitez, "On the functional form of the speed-density relationship—I: General theory," *Transp. Res. Part B Methodol.*, vol. 29B, no. 5, pp. 373–389, Oct. 1995, doi: 10.1016/0191-2615(95)00008-2.
7. J. S. Drake, J. L. Schofer, and A. D. May, "A Statistical Analysis of Speed Density Hypotheses," *Veh. Traffic Sci.*, vol. 154, pp. 112–117, 1967.
8. L. C. Edie, "Car-Following and Steady-State Theory for Noncongested Traffic," *Oper. Res.*, vol. 9, no. 1, pp. 66–76, 1961.
9. H. M. Zhang, "Amathematical theory of traffic hysteresis," *Transp. Res. Part B*, vol. 33, pp. 1–23, 1999.
10. H. Wang, J. Li, Q.-Y. Chen, and D. Ni, "Logistic modeling of the equilibrium speed–density relationship," *Transp. Res. Part Policy Pract.*, vol. 45, no. 6, pp. 554–566, Jul. 2011, doi: 10.1016/j.tra.2011.03.010.
11. D. Ni, J. D. Leonard, C. Jia, and J. Wang, "Vehicle Longitudinal Control and Traffic Stream Modeling," *Transp. Sci.*, vol. 50, no. 3, pp. 1016–1031, Aug. 2016, doi: 10.1287/trsc.2015.0614.

12. R. Kucharski and A. Drabicki, “Estimating Macroscopic Volume Delay Functions with the Traffic Density Derived from Measured Speeds and Flows,” *J. Adv. Transp.*, vol. 2017, pp. 1–10, Feb. 2017, doi: 10.1155/2017/4629792.
13. H. K. Gaddam and K. R. Rao, “Speed–density functional relationship for heterogeneous traffic data: a statistical and theoretical investigation,” *J. Mod. Transp.*, vol. 27, no. 1, pp. 61–74, Mar. 2019, doi: 10.1007/s40534-018-0177-7.
14. M. Y. Mafuyai, D. D. Bakwa, and Y. Y. Jabil, “A Single-Regime Fundamental Diagram of Vehicular Traffic with Excellent Performance at All Traffic States.” 2024. doi: 10.2139/ssrn.4777787.
15. H. Greenberg, “An Analysis of Traffic Flow,” *Oper. Res.*, vol. 7, no. 1, pp. 79–85, Feb. 1959.
16. R. T. Underwood, “Speed, volume and density relationships,” in *Quality and Theory of Traffic flow*, Yale University, New Haven, Connecticut: Bureau of highway Traffic, 1961, pp. 141–188.
17. M. van Aerde, “A single regime speed-flow-density for freeways and arterials,” pp. 1–19, 1995.
18. D. M. Bramich, M. Menendez, and L. Ambuhl, “Fitfun: A modelling framework for successfully capturing the function form and noise of observed traffic flow-density-speed relationships,” *Transp. Res. Part C*, vol. 151, p. 104068, 2023, doi: 10.1016/j.trc.2023.104068.
19. D. M. Bramich, M. Menendez, and L. Ambuhl, “Fitting Empirical Fundamental Diagrams of Road Traffic: A Comprehensive Review and Comparison of Models Using an Extensive Data Set,” *IEEE Trans. Intell. Transp. Syst.*, vol. 23, no. 9, pp. 14104–14127, 2022a, doi: 10.1109/TITS.2022.3142255.
20. A. Romanowska and K. Jamroz, “Comparison of Traffic Flow Models with Real Traffic Data Based on a Quantitative Assessment,” *Appl. Sci.*, vol. 11, no. 21, p. 9914, Oct. 2021, doi: 10.3390/app11219914.